

## **THE EVOLUTION OF DEBONDING IN A SINGLE FIBER COMPOSITE FRAGMENTATION TEST**

R. C. Peterson, G. A. Holmes<sup>\*</sup>, D. L. Hunston, W. G. McDonough

National Institute of Standards and Technology  
Polymers Division  
Gaithersburg, Maryland 20899

### **ABSTRACT**

The performance of a composite is often controlled by the fiber-matrix interface properties and hence they have received considerable attention. One of the techniques used to study the fiber-matrix interface is the single fiber fragmentation test. In this test, the specimen is elongated in tension. As the elongation proceeds, the fiber begins to fragment as its failure strain is exceeded. The fiber fragmentation continues until the fragments are below their critical transfer length, termed saturation. An estimate of the interfacial shear strength is typically derived from the average fiber fragment length at saturation and various micromechanical models. The fiber fragmentation is accompanied by other deformation processes such as matrix cracking and debonding of the matrix from the fiber at the fragment ends. Current micromechanic models often incorporate a debonding parameter to account for the influence of this additional deformation on the resulting interfacial shear strength parameter. Recently, attempts have been made to quantify fiber matrix debonding using the interface energy for the initiation of debonding. However, most of the approaches assume the matrix material to be linear elastic and ignore the contribution of matrix strain on the measured debond length at high stress values. Research at NIST on epoxy/glass specimens indicates that the fragmentation process occurs at strains where the matrix behaves in a non-linear viscoelastic manner. The strain rate in the single fiber fragmentation test was found to influence the fiber fragment distribution and the extent of deformation in the debond regions. These changes in the fragmentation process due to the matrix properties influence the determination of the interfacial shear strength. Measurements of the debond regions indicate the matrix strain can be an order of magnitude higher than the global matrix strain.

### **INTRODUCTION**

Because the fiber-matrix interface plays an important role in the performance of a composite, it has been the focus of much research [1-4]. One parameter of interest is the interfacial shear strength,  $\tau$ , which may be more appropriately described as the ability of the interface to transfer stress between the matrix and fiber. One of the techniques used to probe the interfacial shear

---

<sup>\*</sup> Author to whom correspondence should be addressed.

strength is the single fiber fragmentation (SFF) test. This test has an advantage over other microcomposite tests in that the fiber is loaded in a manner similar to full scale composites and therefore can account for the influence of interfacial pressure from Poisson effects [5]. This paper will discuss the influence of the strain rate and matrix non-linear viscoelasticity on the fragmentation process and the debond regions associated with fiber breaks.

In the SFF test, a dogbone sample of resin is cast with a single fiber embedded down its axis. The matrix should have a higher extension to failure than the fiber. The specimen is loaded in tension and stress is transmitted into the fiber through the fiber-matrix interface. As the strain increases, the stress in the fiber causes it to fail due to inherent flaws in the fiber. As the load increases, this fragmentation process continues until the remaining fiber fragments are too short for sufficient stress to be transferred into the fiber to cause further failure. This point is called saturation. The average fragment length is defined to be  $\frac{3}{4}$  of the critical transfer length,  $l_c$ . The fragment lengths at saturation are measured, and a micromechanics model is used to convert the average fragment length into a measure of the interface strength or stress transfer efficiency.

Several micromechanics models exist to determine the interfacial shear strength with varying built in assumptions. One assumption incorporated in many of the models is the matrix behavior. Early models consider the matrix to be elastic [6] or elastic-perfectly plastic [7]. As a result, the matrix behavior is a constant in the former case and ignored in the latter case. These assumptions can be rather poor for epoxy matrices. Previous research has shown that assuming the matrix is elastic results in interfacial shear strengths that are 15% too high [8]. Consequently, the influence of the matrix behavior on the fragmentation process needs to be incorporated to gain a better understanding of interfacial failure. Numerous efforts are underway to develop better micromechanics models to overcome this and other shortcomings in the assumptions usually made. A detailed examination of the fragmentation process including the debond regions should aid in the development of better models. In this paper, the effect of strain rate on the fragment and debond characteristics will be examined, and the evolution of the fragmentation process will be discussed.

## **EXPERIMENTAL PROCEDURE<sup>a</sup>**

### **MATERIALS**

The matrix material for the single fiber fragmentation specimens was a diglycidyl ether of bisphenol A (DEGBA) epoxy (Epon 828, Shell Chemical Co.) cured with 14.5 phr meta-phenylene diamine (m-PDA) curing agent (Fluka Chemical Co.). The fibers were taken from tows of E-glass (Owens Corning). Each fiber was approximately 15 micrometers in diameter. The tows were shown to have no silane coupling agents or other surface coatings.

---

<sup>a</sup>Certain commercial materials and equipment are identified in this paper in order to specify adequately the experimental procedure. In no case does such identification imply recommendation or endorsement by the National Institute of Standards and Technology, nor does it imply necessarily that the items are the best available for the purpose.

## SPECIMEN PREPARATION

The single fiber dogbone specimens were cast in eight cavity silicone (RTV-664, General Electric) molds. The molds were cured for 24 hours at 23 °C, post-cured for 2 hours at 150 °C and rinsed with acetone prior to use.

Single fibers were extracted from long tows of 30 cm E-glass which had been washed in acetone and dried overnight at 100 °C in a vacuum oven. A single fiber was aligned down the axis of the dogbone cavity of the mold via the sprue slots and temporarily fixed at both ends of the mold with double stick tape. Care was taken to handle only the fiber ends during placement of the fibers. To ensure the fiber was straight, a slight tension was applied while affixing the fiber to the tape. To permanently secure the fibers, drops of 5-minute epoxy mixture were applied at each end of the fiber. This process was repeated until fibers were placed in all eight cavities of each mold.

The m-PDA pellets are melted in a vacuum oven (Fisher Scientific Isotemp Vacuum Oven, Model 281 A) at 75 °C with no vacuum applied. The DGEBA epoxy is also heated in the vacuum oven in a separate beaker. After the m-PDA pellets have completely melted, the m-PDA is added to the epoxy and stirred vigorously manually. The mixture is then degassed in the vacuum oven for approximately 7 minutes.

When melting of the m-PDA pellets was nearly complete, molds containing fibers were placed in an oven (Blue M Stabiltherm, Model OV-560A-2) preheated to 100 °C. The oven was turned off and allowed to cool slowly for approximately 20 minutes. This preheating procedure aids in minimizing voids during the casting process by having the molds at nearly the same temperature as the epoxy mixture. After the epoxy mixture has been degassed, the molds were removed from the oven and the dogbone specimens were cast using 10 cc disposable syringes. The filled molds were then placed in a programmable oven (Blue M, General Signal, Model MP-256-1, GOP), cured for 2 hours at 75 °C, post cured for 2 hours at 125 °C and, allowed to oven cool to room temperature.

## SINGLE FIBER FRAGMENTATION TEST APPARATUS

The single fiber fragmentation test was carried out using a manually operated strain jig similar to that described by Drzal [9] mounted on a polarizing microscope (Nikon Optiphot). The transparent epoxy allowed the fiber to be imaged using transmitted light. The fiber was viewed using a CCD video camera (Optronics LX-450 RGB Remote Head microscope camera) and monitor (Sony, Model PVM-1344Q). The strain jig contained a 2.224 kN load cell, which was connected to a serial port in a computer via a transducer conditioner/digitizer (Cooper Instruments, DA101/AED9001A). The strain jig was also attached to a displacement transducer (LVDT) which allowed the monitoring and recording of position of breaks and other features in the gauge section of the dogbone specimen.

## SINGLE FIBER FRAGMENTATION TEST PROCEDURE

Prior to implementing the loading routine, the specimen cross-sectional dimensions were measured with a micrometer and strain markers, approximately 1 cm apart, were applied to the

center of the gauge section, approximately 1.5 cm long, using a green permanent marker (Staedtler M). The fiber diameter was measured at 19 locations along the gauge length using a pair of crosshairs displayed on a video monitor. The fiber diameter was typically 15 micrometers and the standard uncertainty in the fiber diameter was 0.2 micrometers. To determine the strain, the locations of the strain markers were determined before and after loading by aligning the feature of interest with a crosshair in the microscope and reading the position as given by the LVDT. The fragment and debond lengths were measured using the same procedure as the strain measurements. The standard uncertainty in the instrument for measuring a point was 0.3 micrometers. The standard uncertainty in relocating a point is 1.3 micrometers. The sample dimensions were also measured to calculate the engineering stress. The stress used was the stress 10 s after the peak load was obtained in each strain step. The expected relative standard uncertainty of the load measurement is  $0.03N$ . The standard uncertainty in the measurement of the sample dimensions and the radius of the matrix was 0.005 mm. The expected relative standard uncertainty in the stress measurement is  $0.06\sigma$ . The expected relative standard uncertainty in the strain measurement is  $0.03\epsilon$ . The expected relative standard uncertainty of the fiber strength at the critical length is  $0.03\sigma_f$ . The expected combined relative standard uncertainty of  $\beta$  and the interfacial shear strength,  $\tau$ , is  $0.06\beta$  and  $0.06\tau$ .

The loading procedure consisted of applying a series of small step-strain to the sample. After the application of each step strain, the strain was measured and the sample was held at that nominal strain for a certain period of time depending on the desired strain routine before the next step strain is applied. The average loading time was 1.10 s with a standard uncertainty of 0.2 s and the average displacement was 14.5 micrometers with a standard uncertainty of 3.0 micrometers. Three loading routines were used. The strain was found to increase by  $3.5 \times 10^{-5}$  for each 1 N change in load during the relaxation of the specimen between strain steps. The straining routine was continued until saturation was achieved.

Three straining routines were used to examine the fragmentation process. The first routine allowed the time between strain steps to increase from the initial 10 minutes to over 1 hour depending on the time necessary to make detailed measurements of the fiber fragments and associated debond regions. The second loading routine consisted of a constant 1 hour delay between each strain step. The third strain routine consisted of a constant 10 minute delay between each strain step. This short time delay did not allow detailed measurements of the fragments and debond regions until the end of the test (saturation) when the loading was stopped. The specimen was then unloaded, and the strain allowed to recover. The time required for the strain to recover was at least 5X the time the specimen was under load.

## **RESULTS AND DISCUSSION**

### **STRESS-STRAIN BEHAVIOR**

The stress time profiles are shown in Figure 1 for the three strain routines examined. The times required to reach saturation for these experiments were 5 hrs, 9 hrs, and 25 hrs for the 10 minute strain increment, the variable time strain increment, and the 1 hour strain increment routines, respectively. Figure 2 shows the stress-strain data for the three straining routines. Research by Holmes et al. [13] indicates the nonlinearity of the stress-strain plot is due to the nonlinear viscoelastic behavior of the epoxy matrix. They all achieved saturation at

approximately 4% strain. The three straining routines resulted in different effective strain rates. The effective strain rates were  $2.4 \times 10^{-6} \text{ s}^{-1}$ ,  $1.3 \times 10^{-6} \text{ s}^{-1}$ , and  $4.4 \times 10^{-7} \text{ s}^{-1}$  for the 10 minute strain increment, the variable time strain increment, and the 1 hour strain increment routines respectively. The stress obtained at saturation is similar: 66 MPa and 67 MPa for the 10 minute and variable time strain routines. The stress at saturation was 58 MPa for the 1 hour strain routine due to the greater amount of stress relaxation of the matrix.

## FRAGMENTATION BEHAVIOR

The initial break in the fiber occurred at a slightly higher strain for the 10 minute strain increment routine than for the other straining routines as shown in Figure 3. The maximum fiber stress at  $l_c$  for the three straining routines were 1.9 GPa, 1.7 GPa, and 1.7 GPa, for the 10 minute strain increment, variable time strain increment, and the 1 hour strain increment routines, respectively. These values were calculated using a procedure described by Schultheisz et al [4] assuming a fiber modulus of 72 GPa [10]. The 10 minute and the variable strain routines gave similar stress-strain behavior in the early stages, see Figure 1. The initial fiber breaks in the two cases occur at different strains indicating differences in fiber strengths. The variable and the 1 hour strain routines gave very different stress-strain curves and yet the initial breaks occur at similar strains and indicating similar fiber strengths. The differences in fiber strength may be primarily the result of differences in the inherent flaws in the fibers themselves. The variable and 1 hour strain routines were at a high stress level for much longer than the 10 minute strain routine, which may have resulted in a decrease in the fiber strength, if static fatigue of the plays a significant role.

As shown by Figure 3, the number of breaks increases with strain reaching a plateau level termed saturation. The fragmentation process can be examined through the use of a fragmentation map shown in Figure 4. The fragmentation map shows the location of breaks along the fiber and charts the progression of the fragmentation process with increasing global strain. The fiber is represented by two closely spaced horizontal lines. Seventeen different strain steps are included in the figure, one above the other. The breaks are indicated by vertical lines through the fiber. To better visualize the break pattern that develops, each new fiber is translated and scaled so that the corresponding breaks align vertically. The scaling factors provide an alternative way to determine the relative global strain once a number of breaks are present. The strain and number of breaks are indicated at the right side of Figure 4. The strain determined from the program used to generate the fragmentation map agreed to within 0.0001 of that measured directly from the strain markers on the sample. As the fiber fragments, the breaks are accompanied by some debonding of the matrix along the fiber ends as shown by Figure 5. The debond areas appear as black regions in the optical microscope. Within this black region are the ends of the fiber fragments. It is assumed that the matrix is no longer chemically bonded to the fiber within these regions and therefore little stress can be transferred across the interface. Birefringence bands under polarized light appear to end at the edge of the debond regions as shown in Figure 5 and supports the idea that there is little stress transfer occurring in the debond regions.

The fiber fragments were measured from the edge of one debond region to the start of the next. Only in these bonded regions (i.e. outside of the black regions) can significant stress be transferred and play a role in the further fragmentation of fiber lengths greater than the critical

length. The debond regions were measured to monitor changes with global strain as the specimen approached saturation. The average fiber fragment and debond lengths at saturation are shown in Table I for the three loading routines examined. These lengths were measured from grip to grip, but only the gauge section of the dogbone samples where the displacement transducer yielded reliable values were used in any analysis. The sampling lengths were 16.11 mm, 15.89 mm, and 15.79 mm for the 10 minute, the variable, and the 1 hour strain routines, respectively. The number of fragments and debonds analyzed was from 40 to 46 depending on the straining routine.

The average fragment lengths at saturation under load were 375  $\mu\text{m}$ , 361  $\mu\text{m}$ , and 326  $\mu\text{m}$  for the 10 minute, the variable, and the 1 hour strain routines, respectively. The standard deviations were 94  $\mu\text{m}$ , 97  $\mu\text{m}$ , and 79  $\mu\text{m}$  respectively. The 10 minute and the variable strain routines had similar average fragment lengths, while the 1 hour straining routine resulted in a shorter average fragment length. The fragment lengths decreased only slightly after the stress was removed and the samples were allowed to relax. The average fragment lengths in the relaxed state were 370  $\mu\text{m}$ , 359  $\mu\text{m}$ , and 321  $\mu\text{m}$  respectively. The distribution of the fiber fragment lengths at saturation under stress and no stress are shown in Figures 6 and 7. In Figure 6, both the 10 minute and variable straining routines resulted in a skewed distribution with a tail at longer fiber fragments. The 1 hour straining routine produced a normal distribution with no long fragment tail. A single factor analysis of variance (ANOVA) of the fragment distributions found no statistical significant difference between the 10 minute and variable straining routines ( $F = 0.67 < F_{\text{crit}} = 2.68$ , P-value of 0.56). There was a significant difference between the variable and the 1 hour strain routines ( $F = 4.23 > F_{\text{crit}} = 2.68$ , P-value of 0.015).

The average lengths of the debond regions at saturation under load were 26  $\mu\text{m}$ , 23  $\mu\text{m}$ , and 23  $\mu\text{m}$  for the 10 minute, the variable time, and the 1 hour strain routines, respectively. The standard deviations were 3.9  $\mu\text{m}$ , 2.4  $\mu\text{m}$ , and 2.5  $\mu\text{m}$ , respectively. The average debond length did decrease significantly when the stress was removed, and the matrix allowed to relax. The debond lengths at saturation under no stress were 18  $\mu\text{m}$ , 16  $\mu\text{m}$ , and 15  $\mu\text{m}$ , respectively. The distribution of the debond lengths at saturation under stress and no stress are shown in Figures 8 and 9. The straining routine had little influence on the debond lengths. The single factor ANOVA of the debond distributions within the variable time straining and comparing the variable time and both the 10 minute and the 1 hour strain resulted in F- values  $> 12$  and corresponding P-values  $< 10^{-5}$ . Therefore the debond distributions are not a function of the straining routines, but probably relate to the flaw distribution of the fibers and variations in the cross-link density of the matrix. There was a significant shift in the average debond length when the stress was removed, but the distribution profile remained essentially the same.

The large change in the average debond lengths after the stress was removed indicates the matrix is under a large amount of strain. It has been proposed that the fiber fragmentation releases much more energy than can be accounted for by the energy absorbed by the debonding at the fiber fragment ends [11]. This additional energy goes into the deformation of the cylinder of matrix surrounding the debond regions. The global strains in the samples at saturation under stress were 0.0438, 0.0404, and 0.0437 for the 10 minute, the variable, and the 1 hour straining routines, respectively. The corresponding average strains measured for the fiber fragments at saturation under stress were 0.0212, 0.0192, and 0.0194, respectively. The debond strains, however, were much larger. The average debond strains were 0.425, 0.439, and 0.472, respectively. Because the debonds represent such a small total length (debond lengths range from 15 to 30  $\mu\text{m}$ ), they should be under a large amount of strain so that the addition of individual

fragment and debond strains correspond to the global strain. The strains in the debond regions are much higher than the failure strain of approximately 0.10 for dogbones of matrix only. These large deformations in localized regions have been observed in composites previously[12]. These high strains represent yielding of the matrix in the debond regions as represented by the residual strain after the stress has been removed. The residual strain in the specimen, after removal of the stress and suitable relaxation time, was influenced by the effective strain rate of the straining routines. The residual strains were 0.0043, 0.0027, and 0.0011 for the 10 minute, the variable, and the 1 hour straining routines respectively. Perhaps the longer time between strain steps during the 1 hour test allowed the matrix to dissipate the strain over a larger volume of matrix. As the strain rate increased, there was not sufficient time for this process to occur resulting in greater permanent deformation of the matrix surrounding the debond regions. This localized yielding around the debond regions may result in some stiffening of the specimen due to orientation of the chains and could explain the increase in the tangent modulus of a SFFT sample relative to a dogbone of matrix only[13].

The location of fiber breaks and the associated debond regions occur according to the distribution of fiber flaws as the sample is strained. From the fragmentation map in Figure 4, the initial debond regions can be far apart spatially. As the fragmentation process continues, debond regions are generated near existing debond regions. Longer fragments were observed to have higher strains than shorter fragments. As these longer fragments continue to fracture, more debond regions are created which increase the strain in the softer matrix resulting in a decrease of the strain the fragment. The global strain does not get transmitted along the sample uniformly as breaks begin to occur. The change in the average debond length with increasing strain is shown in Figure 10 for a sample which underwent the variable strain routine. The average debond length generally increases with strain, but several drops in length can be observed. These drops are the result of numerous additional breaks occurring during the next strain step which absorb the strain not only from the fiber fragments, but also from nearby debond regions. This is shown clearly in Figure 10 for a particular debond region. Sharp drops in length are observed when additional breaks form nearby. The distance at which the debond regions interact appears to be fairly small, approximately 0.5 mm. The interaction of the debond regions can be observed for fragments just greater than the critical fragment length. A break in such a fragment results in a debond region only approximately  $\frac{1}{2}$  the length of the neighboring debond regions. This may suggest that the strain is absorbed quickly in the adjacent debond regions reducing the driving force for the deformation in the new debond region. The evolution of the fragmentation process could not be monitored for the 10 minute strain increment routine as the time between successive strain steps was not sufficient to manually measure the fragments and debonds. At saturation, the fragment and debond strain profiles along the gauge section were measured for all the straining routines. These profiles were found to be similar for all three straining routines. The fragment and debond strain profiles along the central gauge section are shown in Figure 11 for a sample which underwent the variable strain routine. Fragments with higher strains are associated with debond regions on either side of lower strain while fragments with lower strains have debond regions adjacent to them of high strains. The sharp peaks and valleys illustrate that the strain is not distributed along the sample uniformly.

## INTERFACIAL SHEAR STRENGTH

The interfacial shear strength can be calculated from the average fragment lengths at saturation and the fiber strength at the critical length. The interfacial shear strength,  $\tau_{\max}$ , was determined using a modified Cox model [13] with the following form:

$$\tau_{\max} = \frac{d_f \cdot \beta}{4} \left( \frac{\sinh\left(\frac{\beta \cdot l_c}{2}\right)}{\cosh\left(\frac{\beta \cdot l_c}{2}\right) - 1} \right) \sigma(l_c)$$

where  $d_f$  is the fiber diameter,  $l_c$  is the fiber critical length taken to be 4/3 the average fiber fragment length at saturation,  $\sigma(l_c)$  is the fiber strength at the critical length and  $\beta$  is given by the following expression:

$$\beta = \frac{2}{d_f} \left[ \frac{E\{\epsilon, t\}_{\text{sec ant}}}{(1 + \nu_m) \cdot (E_f - E\{\epsilon, t\}_{\text{sec ant}}) \cdot \ln\left(\frac{2 \cdot r_m}{d_f}\right)} \right]^{1/2}$$

where  $\nu_m$  is Poisson's ratio for the matrix ( $\nu_m = 0.35$  [14]),  $r_m$  is the radius of the matrix taken to be 1/2 the specimen thickness in the absence of direct measurements, and  $E\{\epsilon, t\}$  is the secant modulus of the matrix. The modified Cox model uses the secant modulus for the matrix as a conservative approximation to account for the nonlinear viscoelastic behavior shown in Figure 2. The fiber fragmentation occurs in the nonlinear region and therefore the elastic matrix typically used is not appropriate. The interfacial shear strengths determined for the 10 minute, the variable time and 1 hour straining routines were 74.0 MPa, 72.5 MPa. and 70.5 MPa, respectively. See Table II.

## CONCLUSIONS

The matrix behavior exhibits pronounced nonlinear viscoelastic behavior over the strain range where the fragmentation process occurs for the strain rates examined. The effective strain rate did not influence the calculated interfacial shear strength. The effective strain did influence the fiber fragmentation distribution, but not the debond distribution. The slowest strain rate resulted in the shortest average fragment length and the narrowest distribution. The increase in the measured debond lengths with strain may be the result of deformation of the matrix. The debond regions have strains ranging from 0.20 to 0.50 while the fiber fragment strains range from 0.01 to 0.02. The majority of the strain in the debond regions could be recovered by releasing the stress on the sample. The slowest strain rate did result in the smallest residual strain at saturation after the stress was relaxed. The results suggest that there is an interaction between

the fragments and debonds resulting in a local adjustment of the strain during the fragmentation process. This interaction seems to extend over only short lengths, perhaps 0.5 mm to 0.75 mm. Much of the strain in the fragments appears to transfer to the debond regions during fragmentation. Fragments with lower than average strains have debond regions at either end with higher than average strains.

The deformation in the debond regions needs to be included in the models of the fragmentation process. An automated method to observe the fragmentation process at high strain rates is necessary if detailed information of the debond region is to be obtained and their influence on the fragmentation process determined. Additional experiments are necessary to examine the significance of these results and to understand the fragmentation process more completely.

## REFERENCES

1. McKenna, G. B., "Interlaminar Effects in fiber reinforced Plastics-A Review," *Polymer Plast. Tech.* **5**(1), 23-53 (1975)
2. Madukar, M. S. and Drzal, L. T., "Fiber-Matrix Adhesion and Its Effects on Composite Mechanical Properties: I. In Plane and Interlaminar Shear Behavior of Graphite/Epoxy Composites," *J. Compos. Mater.*, **25**, 932-956 (1991)
3. Madukar, M. S. and Drzal, L. T., "Fiber-Matrix Adhesion and Its Effects on Composite Mechanical Properties: II. Longitudinal (0) and Transverse (90) Tensile and Flexural Behavior of Graphite/Epoxy Composites," *J. Compos. Mater.*, **25**, 932-956 (1991)
4. Schultheisz, C. R., McDonough, W. G., Kondagunta, S., Schutte, C. L., Macturk, K. S., McAuliffe, M., and Hunston, D. L., "Effect of Moisture on Glass/Epoxy Interfacial and Fiber Strengths," in *ASTM Symposium on Composite Materials: Testing and Design*, ASTM STP-1242 (ASTM, West Conshohocken, PA) 257-286 (1997)
5. Piggott, M. R., "Failure Processes in Fibre-Polymer Interphase," *Compos. Sci. and Tech.*, **42**, 57-72 (1991)
6. Cox, H. L., "The Elasticity and Strength of Paper and Other Fibrous Materials," *Brit. J. of Applied Physics*, **3**, 72-79 (1952)
7. Kelly, A., and Tyson, W. R., "Tensile Properties of Fibre-Reinforced Metals: Copper/Tungsten and Copper/Molybdenum" *J. Mech. Phys. Solids*, **13**, 329-350 (1965)
8. Feillard, P., Desarmot, G., and Favre, J. P., "A Critical Assessment of the Fragmentation Test for Glass/Epoxy Systems," *Compos. Sci. and Tech.* **49**, 109-119 (1993)
9. Drzal, L. T., Herrera-Franco, P. J., "Composite Fiber-Matrix Bond Test," in *Engineered Materials Handbook: Adhesive and Sealants*, Vol. 3, (ASM International, Metals Park, OH) 391-405 (1990)

10. Lowrie, R. E., "Glass Fibers for High Strength Composites," in Modern Composite Materials, (Addison-Wesley Publishing, Reading, MA) Broutman-Krock Eds., 281 (1967)
11. Nairn, J. A., and Liu, Y. C., "On the use of energy methods for interpretation of results of single-fiber fragmentation experiments," *Comp. Interfaces*, 4(5), 241-267 (1997)
12. Bascom, W. D., Boll, D. J., Hunston, D. L., Fuller, B. and Phillips, P. J., "Fractographic Analysis of Interlaminar Fracture," Toughened Composites, ASTM STP 937, (ASTM, Philadelphia, PA), 131-149, (1987).
13. Holmes, G. A., Peterson, R. C., Hunston, D. L., and McDonough, W. G., "The Effect of Nonlinear Viscoelasticity on Interfacial Shear Strength Measurements," ASTM STP-1357 (ASTM, West Conshohocken, PA) in press
14. Whitney, J., and Drzal, L., "Axisymmetric Stress Distribution Around an Isolated Fiber Fragment," Toughened Composites, ASTM STP 937, (ASTM, Philadelphia, PA), 179-196, (1987)

Table I

Average Fragment and Debond Lengths at Saturation Under Stress

	10 Minute Strain Increment		Variable Time Strain Increment		1 Hour Strain Increment	
	Fragment (μm)	Debond (μm)	Fragment (μm)	Debond (μm)	Fragment (μm)	Debond (μm)
Average	374.5	26.1	360.7	23.4	326.0	22.8
St. Dev.	94.0	3.9	97.2	2.4	78.5	2.5

Table II

Values Used in Equations 1 and 2 to Determine Interfacial Shear Strength

	10 Minute Strain Increment	Variable Time Strain Increment	1 Hour Strain Increment
Fiber Modulus (GPa)	72	72	72
Poisson's Ratio	0.35	0.35	0.35
Fiber Strength at the Critical Length (GPa)	1.9	1.7	1.7
Specimen Thickness (mm)	1.54	1.43	1.3
Radius of the Matrix (mm)	0.77	0.72	0.65
Fiber Diameter (mm)	0.01499	0.01607	0.01474
Critical Fiber Length at Saturation (mm)	0.4993	0.4809	0.4347
Secant Modulus of the Matrix at Saturation (GPa)	1.509	1.666	1.375
$\beta$ (mm <sup>-1</sup> )	7.806	7.776	7.700
Interfacial Shear Strength (MPa)	74.0	72.5	70.5

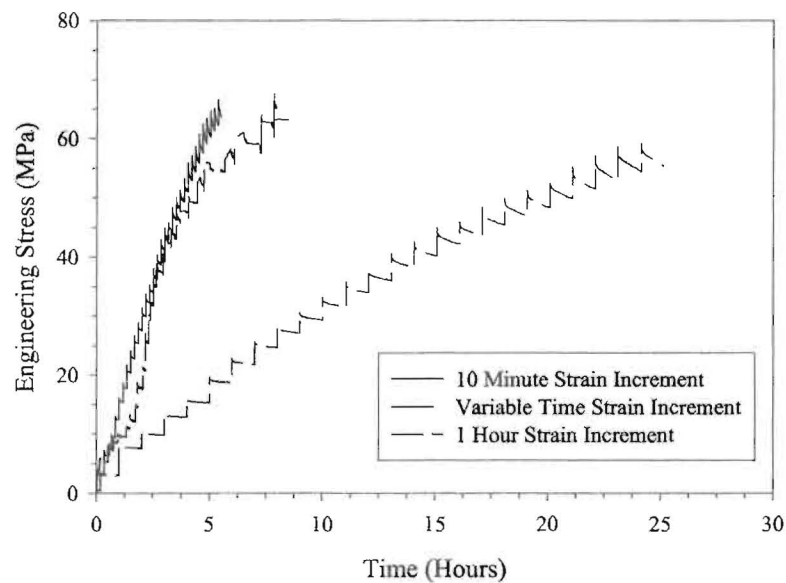


Figure 1. Stress versus time for the three strain routines examined: 10-minute strain increments, variable time strain increments, and 1 hour strain increments.

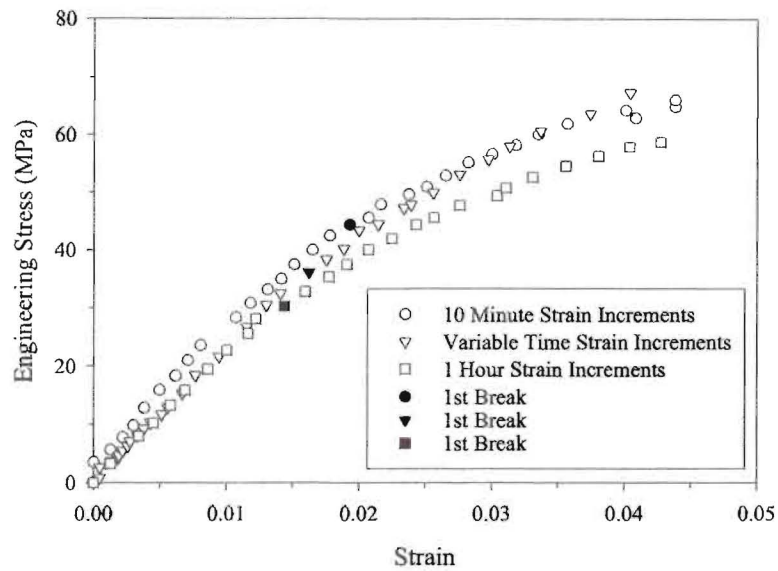


Figure 2. Stress at 10 s after each strain increment versus strain for the three straining routines. Closed Symbols indicate strain at which the initial break occurred.

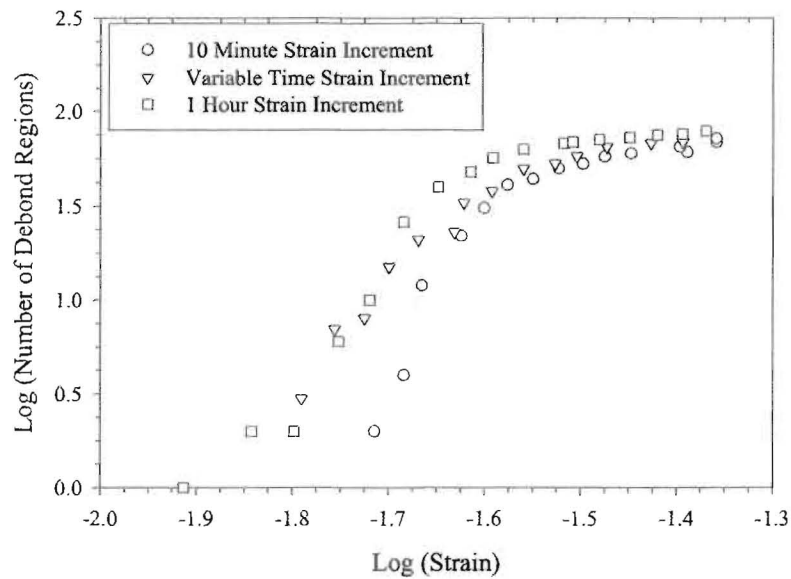


Figure 3. Plot of log(debond regions) versus log(strain) to determine fiber strength near the critical length.

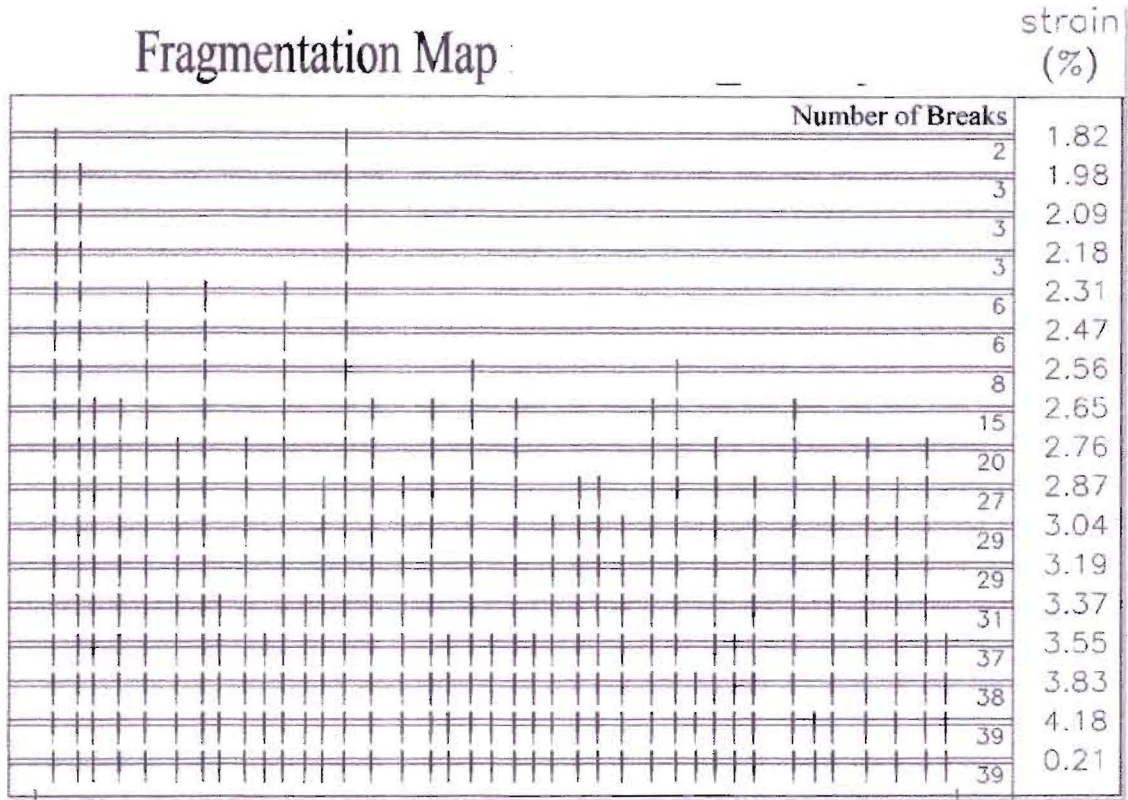


Figure 4. Fragmentation map for the variable time strain increment routine.

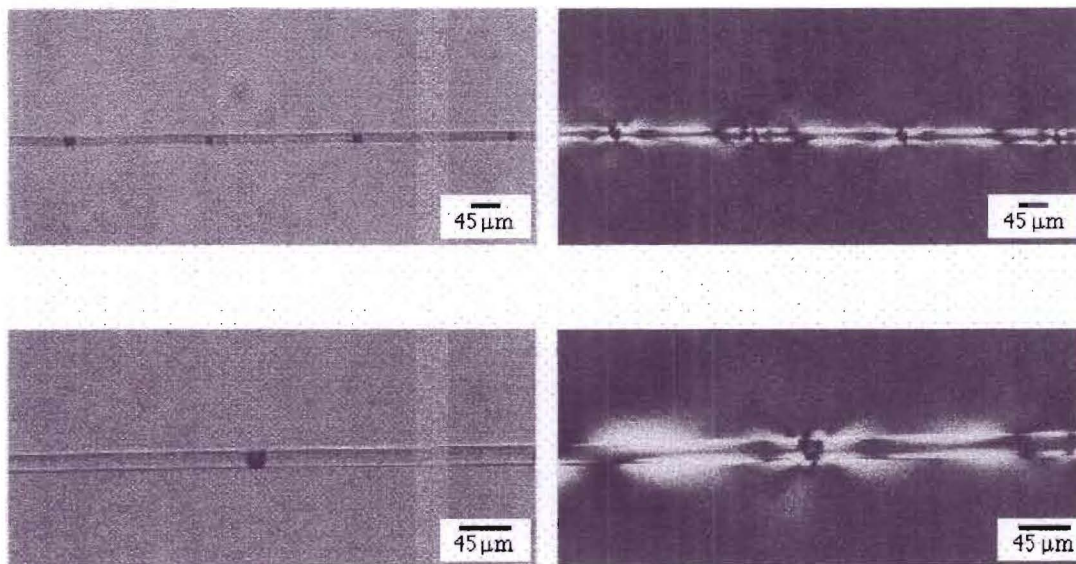


Figure 5. Image of the fragments and associated debond regions.

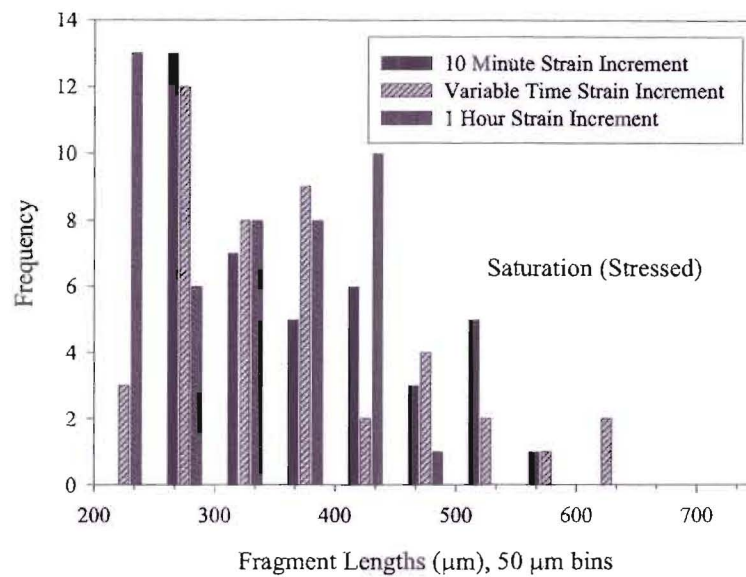


Figure 6. Fragment distributions at saturation under stress for the three straining routines.

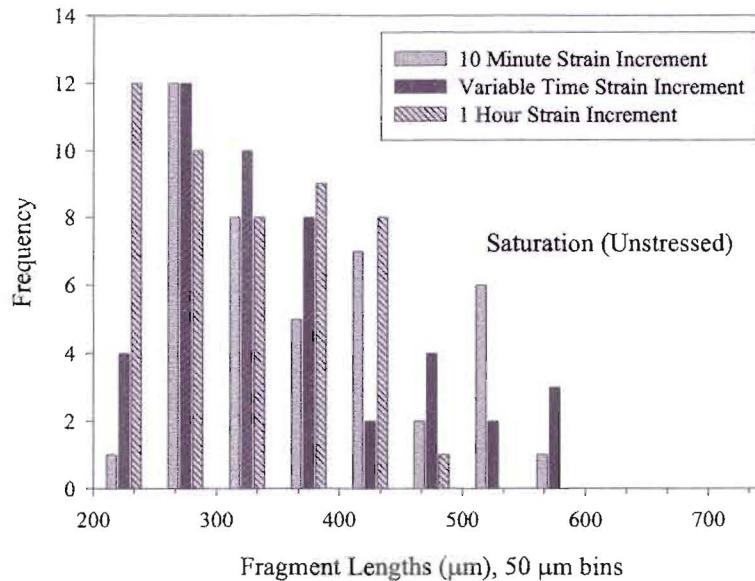


Figure 7. Fragment distributions at saturation under no stress for the three straining routines.

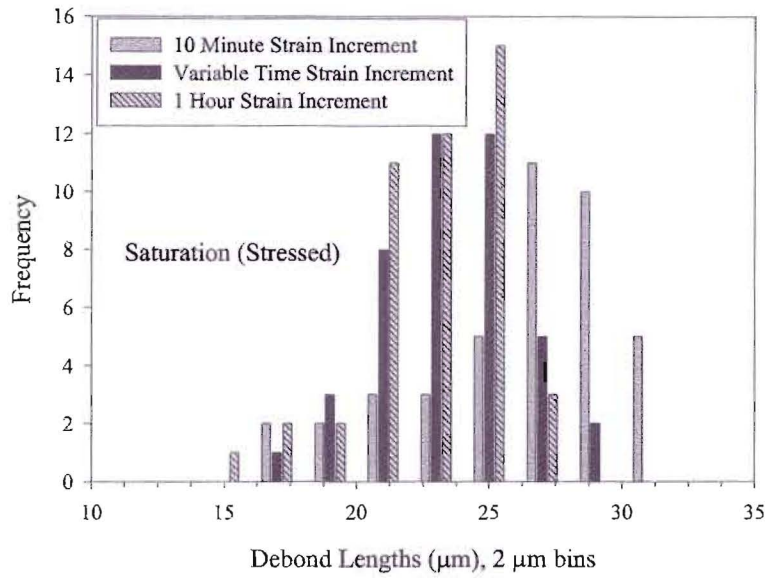


Figure 8. Debond distributions at saturation under stress for the three straining routines.

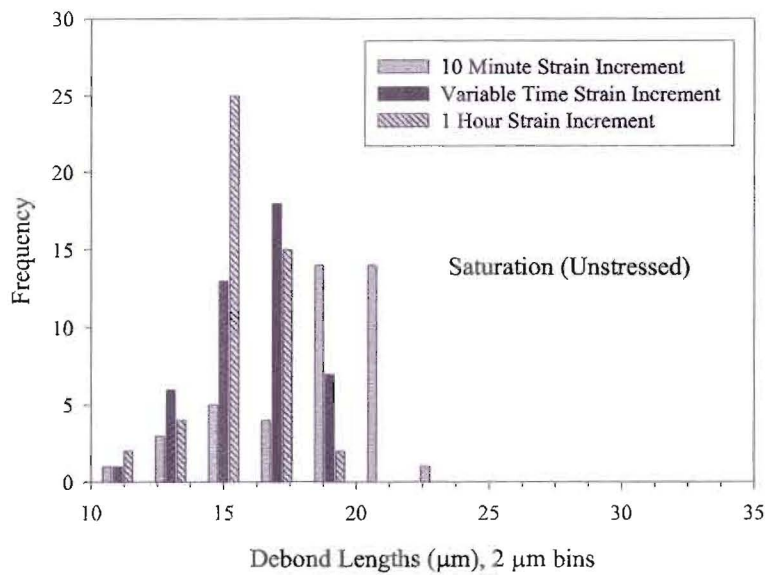


Figure 9. Debond distributions at saturation under no stress for the three straining routines.

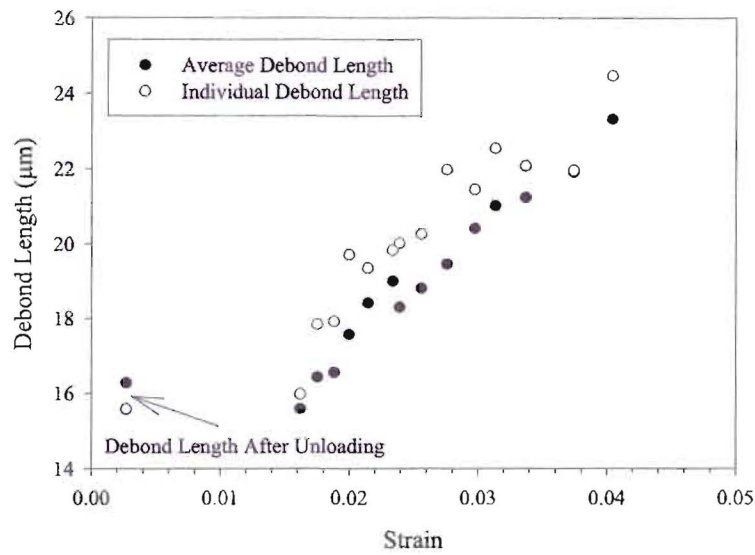


Figure 10. Changes in debond length with increasing strain for the variable time strain routine.

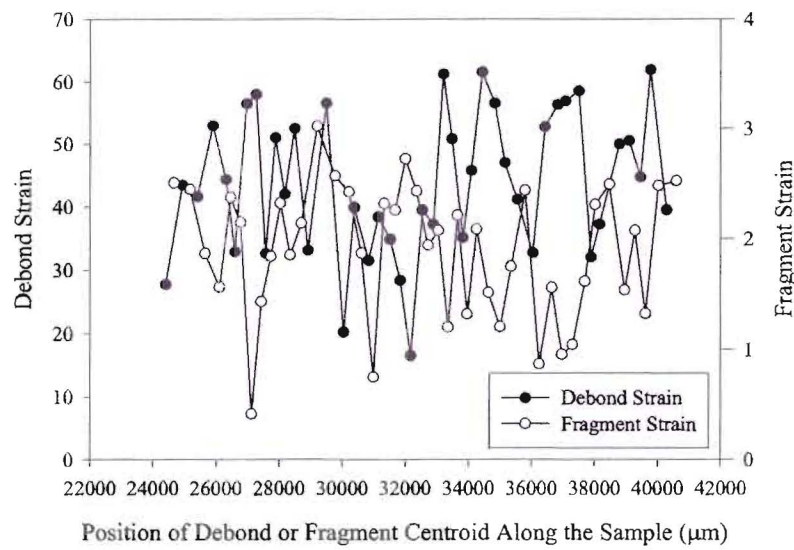


Figure 11. Fragment and debond strain along the gauge length.